Phase Turbulence and Heteroclinic Cycles

F.H. Busse, O. Brausch, M. Jaletzky and W. Pesch

Abstract
Various cases of phase turbulence in convection layers heated from below are reviewed. In several cases a close connection between the onset of phase turbulence and the existence of a heteroclinic orbit in a reduced system of equations can be found. New results are presented for phase turbulence in the case of centrifugally driven convection in a rotating cylindrical annulus.

1 Introduction

Phase turbulence is observed in many extended fluid systems that are characterized by supercritical or only weakly subcritical bifurcations from the uniform basic static state under steady external conditions. A large number of bifurcating solutions usually exists in the neighborhood of the critical value of the control parameter and the mathematical problem can be considered as an unfolding from a bifurcation point of infinite codimension. In the absence of a variational principle guaranteeing a unique asymptotic state the competing modes often give rise to a spatio-temporally complex state. In particular the phases of the flow at a given location appear to vary in a chaotic fashion.

The standard methods for analyzing pattern forming instabilities apply to large aspect-ratio systems, which can be idealized as infinitely extended. Therefore a description in terms of Fourier modes in dependence on two-dimensional wave vectors $\boldsymbol{k}$ is natural. In particular near onset of convection, i.e. when the main control parameter R, such as the Rayleigh number in Rayleigh–Bénard convection, is slightly beyond its critical value, almost perfect periodic patterns like rolls (characterized by a single wave vector), but also squares (two distinct wave vectors) or hexagons can be obtained. Besides the nearly periodic pattern, experiments often exhibit persistent spatio-temporal dynamics. Snapshots of the patterns in this case show local roll patches corresponding to wave vectors varying with respect to their direction while the absolute values of the wave vectors are nearly constant. The discontinuities in the wave vector field like grain boundaries or immersed point defects (dislocations) trigger the dynamics of the patterns. The notion 'phase turbulence' or 'weak turbulence' has been introduced for such states in distinct contrast to more fully developed turbulence.

Properties of Turbulence

Chaotic time dependence	Decay of spatial correlations	Broad wavenumber spectrum	Inertial range, fractal structure
Dynamical Systems few degrees of freedom, e.g. convection in a box			
Phase Turbulence many degrees of freedom, nearly degenerate bifurcation, e.g. convection in extended layers with rotation			
Classical Turbulence Interaction with boundaries, e.g. turbulent pipe and channel flow; thermal convection at high Rayleigh numbers			
Asymptotic Turbulence Inertial range scaling, e.g. atmospheric flows and other high Reynolds number systems			

Table 1

Phase turbulence is thus a phenomenon that exhibits certain properties of fluid turbulence while others are missing. The reduced complexity of phase turbulent systems can therefore provide examples in which certain aspects of fluid turbulence can be studied in a relatively simple setting. Table 1 may serve to illustrate the place of phase turbulence within the general field of fluid turbulence.

One way of elucidating the mechanism of phase turbulence is the exploration of the stability of periodic patterns in the R-$\boldsymbol{k}$-space. In fact, in the most important and representative cases phase turbulence originates from the nonexistence of stable periodic states immediately above onset. Historically the first example has been convection in a rotating Rayleigh–Bénard layer. Küppers and Lortz (1969) realized that all steady solutions describing convection flows in a horizontal fluid layer heated from below and rotating about a vertical axis are unstable when the rotation parameter Ω exceeds a critical value. They concluded that some kind of turbulent motion must be realized as a result. In later studies a close connection of the time-dependent states with a heteroclinic orbit was recognized (Busse and Clever, 1979a) and simple models based on this idea (Busse, 1984) could explain the experimental observations (Busse and Heikes, 1980; Heikes and Busse, 1980) quite well. Since then the system of rotating convection has become a favored example for the study of spatio-temporal chaos in pattern forming systems. Both experimental investigations (Zhong *et al.*, 1991; Zhong and Ecke, 1992; Bodenschatz

et al., 1992; Hu *et al.*, 1995, 1997, 1998) and numerical simulations (Tu and Cross, 1992; Fantz *et al.*, 1992; Neufeld and Friedrich, 1995; Millán-Rodriguez *et al.*, 1995; Pesch, 1996; Ponty *et al.*, 1997) have been employed to study various aspects of this phase turbulent system.

In the meantime other systems exhibiting phase turbulence were found. Zippelius and Siggia (1982) showed that Rayleigh–Bénard convection in a non-rotating layer with stress-free boundaries also exhibits the property that none of the existing infinite steady solutions is stable for sufficiently low Prandtl numbers and as a consequence phase turbulence must be expected. The mathematical analysis of Zippelius and Siggia was based on incorrect assumptions, but a later, more general analysis of Busse and Bolton (1984) confirmed that all solutions are indeed unstable albeit through different mechanisms of instability. The resulting phase turbulence has been studied in various papers (Busse, 1986; Busse and Sieber, 1991; Busse *et al.*, 1992; Xi *et al.*, 1997). But, unfortunately, there exists no possibility for a direct comparison with experiments since stress-free boundaries can be realized only for fluid layers with large Prandtl numbers (Goldstein and Graham, 1969).

Another system in which spatio-temporal chaos is easily observable is electroconvection in a layer of nematic liquid crystals. For experimental and theoretical studies of this system we refer to a recent review by Pesch and Behn (1998). Of special interest are cases where the primary bifurcation from the spatially homogeneous state occurs in the form of an oscillatory instability giving rise to traveling waves at threshold. It can happen that none of these wave states is stable owing to the Benjamin–Feir instability resulting in spatio-temporally disordered patterns (Dangelmayr and Kramer, 1998). Less well understood are the situations where phase turbulence cannot be related to an instability such as spiral defect chaos which has attracted much attention in recent years (Morris *et al.*, 1993).

It is common to make a distinction between phase turbulence and defect turbulence. The latter is characterized by the persistent spontaneous creation and extinction of defects which are defined as points where the phase jumps by 2π while the amplitude vanishes in an otherwise smooth pattern. But since experimentally realized phase turbulence is always associated with certain kinds of defects and grain boundaries, it is difficult to sustain the distinction for physical systems. The two ideal cases of spatio-temporal chaos generated solely by defects corresponding to phase singularities and the spatio-temporal chaos associated with entirely smoothly varying phase can be regarded as extreme cases of various possibilities for turbulence close to the critical value of the control parameter.

In the following we shall first discuss briefly the cases of variational and non-variational dynamics in Rayleigh–Bénard layers and then focus in the third section on the role of heteroclinic orbits. In the fourth section the newly

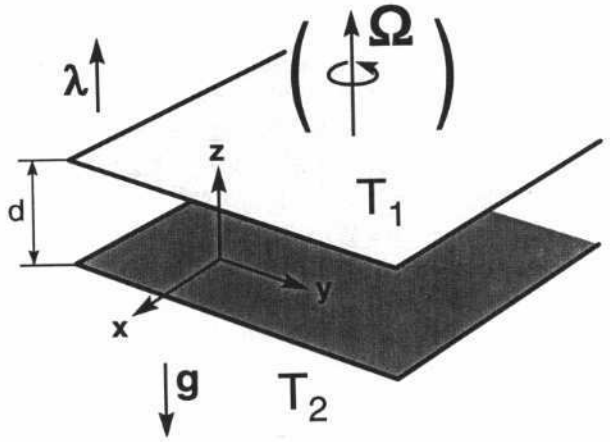

Fig. 1: Sketch of a horizontal fluid layer heated from below and possibly rotating about a vertical axis.

studied case of a Rayleigh–Bénard layer with 'horizontal' axis of rotation will be presented in which heteroclinic cycles also play a role. The paper closes with some concluding remarks in section 5.

2 Variational and Non-Variational Dynamics in Rayleigh–Bénard Convection

We consider a horizontal, infinitely extended fluid layer of height d heated from below as shown in figure 1. Because of the horizontal isotropy the onset of convection corresponds to a bifurcation of infinite codimension. The general solution of the linearized basic equations (see, for example, Busse, 1978) can be written in the form

$$w = f(z,\alpha) \sum_{n=-N}^{N} C_n \exp\{i\boldsymbol{k}_n \cdot \boldsymbol{r}\} \tag{2.1a}$$

where the conventions

$$C_n = C_{-n}^{+}, \quad \boldsymbol{k}_{-n} = -\boldsymbol{k}_n, \quad |\boldsymbol{k}_n| = \alpha, \quad \boldsymbol{k}_n \cdot \boldsymbol{\lambda} = 0 \quad \text{for all } n \tag{2.1b}$$

have been used and where a Cartesian system of coordinates (x, y, z) with z in the vertical direction has been assumed; $\boldsymbol{\lambda}$ is the vertical unit vector and C^{+} denotes the complex conjugate of C. Expression (2.1a) is given for the vertical velocity component. Analogous expressions hold for the other variables such as the temperature field. A special role is played by the regular distributions of $\boldsymbol{k}$-vectors for which all angles φ between neighboring vectors $\boldsymbol{k}_n$ assume the same value, $\varphi = \pi/N$. Patterns which are periodic in the

plane are obtained in the special cases $N = 1, 2, 3$ which correspond to rolls (or stripes), squares and hexagons, respectively. In the general case N may tend to infinity in which case functions of the form (2.1) correspond to the class of almost periodic functions in the x-y-plane with fixed wavenumber.

The control parameter of the problem is the Rayleigh number R which is proportional to the applied temperature difference between bottom and top of the layer and which assumes a minimum as a function of wavenumber α for $\alpha_c = 3.116/d$ and $\alpha_c = \pi/d\sqrt{2}$ in the cases of no-slip and stress-free conditions at the boundaries, respectively. The corresponding critical values of the Rayleigh number are $R_c = 1707.76$ and $27\pi^4/4$. A solution of the form (2.1) is also obtained when the layer is rotating about a vertical axis, since it is possible to design experiments such that the centrifugal force is negligible while the Coriolis force plays an important role.

The arbitrary choice of the amplitudes C_n becomes restricted when the nonlinear problem is considered. For example, $|C_1|^2 = |C_2|^2 = \cdots = |C_N|^2$ must be satisfied for steady solutions corresponding to regular distributions of the vectors $\boldsymbol{k}_n$. These constraints on the coefficients C_n are obtained from the solvability conditions in the cubic order of the expansion of the basic equation in powers of the amplitude of convection. More general constraints are obtained when a time dependence of the coefficients on a long time scale is admitted. The solvability conditions give rise to evolution equations for the amplitudes $C_n(t)$ of the form

$$\frac{d}{dt}C_j^+ = (R - R_0)KC_j^+ + \beta \sum_{n,m=-N}^{N} C_n C_m \delta(\boldsymbol{k}_j + \boldsymbol{k}_n + \boldsymbol{k}_m)$$

$$- \left[\sum_{n=1}^{N} |C_n|^2 A(\boldsymbol{k}_j \cdot \boldsymbol{k}_n) + \underline{\Omega E(\boldsymbol{k}_j \cdot \boldsymbol{k}_n)\ \boldsymbol{\lambda} \cdot \boldsymbol{k}_j \times \boldsymbol{k}_n}\right] C_j^+$$

$$\underline{+iM\nabla\psi \times \boldsymbol{\lambda} \cdot \boldsymbol{k}_j C_j^+} \qquad \text{for} \quad j = -N, \ldots, N, \quad (2.2a)$$

$$\underline{\left(\frac{\partial}{\partial t} - \frac{\partial^2}{\partial x^2} - \frac{\partial^2}{\partial y^2}\right)\psi = \sum_{r,p} \hat{q}_{rp} C_r C_p \exp\{i(\boldsymbol{k}_r + \boldsymbol{k}_p) \cdot \boldsymbol{r}\}.} \qquad (2.2b)$$

Here K, β and M are constants while A and E are functions of $\boldsymbol{k}_i \cdot \boldsymbol{k}_n$ and β provides a measure for deviations from the Boussinesq approximation, i.e. for the temperature dependence of the viscosity etc., which tend to favor hexagonal convection cells. The terms underlined by a solid line enter the problem only in the case of stress-free boundary conditions in which case a z-independent mean flow described by a slowly varying stream function $\psi(x, y, t)$ can be generated. The term proportional to Ω and underlined by a dashed line enters the problem only in the case of a rotating layer where $\Omega = \Omega_D d^2/\nu$ is the rotation parameter made dimensionless with the thickness

d of the layer and the kinematic viscosity ν of the fluid. Ω_D is the dimensional angular velocity of rotation. Because the reflection symmetry of the basic equations with respect to vertical planes is lost in a rotating system, terms proportional to $\boldsymbol{\lambda}\cdot\boldsymbol{k}_j\times\boldsymbol{k}_n$ enter in addition to those depending only on inner products $\boldsymbol{k}_j\cdot\boldsymbol{k}_n$ between $\boldsymbol{k}$-vectors. Without the underlined terms the right hand side of expressions (2.2a) can be written as derivatives of a Lyapunov functional $F(C_{-N},\ldots,C_N)$,

$$\frac{d}{dt}C_j^+ = -\frac{\partial}{\partial C_j}F(C_{-N},\ldots,C_N) \qquad \text{for } j=-N,\ldots,N \tag{2.3a}$$

with

$$\begin{aligned} &F(C_{-N},\ldots,C_N)\\ &\quad\equiv -\frac{1}{2}(R-R_0)K\sum_{j=-N}^{N}|C_j|^2-\frac{1}{3}\beta\sum_{j,n,m}C_jC_nC_m\delta(\boldsymbol{k}_j+\boldsymbol{k}_n+\boldsymbol{k}_m)\\ &\qquad+\frac{1}{4}\sum_{n,j}A(\boldsymbol{k}_j\cdot\boldsymbol{k}_n)|C_n|^2|C_j|^2. \end{aligned} \tag{2.3b}$$

The variational dynamics expressed by these equations guarantees the existence of at least one stable stationary solution of the problem corresponding to a minimum of the functional F. But, of course, there may be more than one attractor corresponding to more than one local minimum of F, as happens in the case of the competition between rolls and hexagonal convection cells (Busse, 1967).

The property (2.3) disappears in problems of Rayleigh–Bénard convection with rotation about a vertical axis or with stress-free boundaries and indeed it can be demonstrated that all steady solutions are unstable if either Ω is sufficiently large (Küppers and Lortz, 1969) in the former case or the Prandtl number P is less than 0.543 in the case of stress-free boundaries (Busse and Bolton, 1984; see also Mielke, 1997). In other cases of Rayleigh–Bénard convection the steady attracting flow also does not remain stable as the Rayleigh number R is increased much beyond the critical value due to higher order terms which can no longer be neglected in equations (2.2). But except for the two special cases mentioned above there always exists a region close to the critical value of the Rayleigh number where the variational dynamics described by equations (2.3) is applicable.

3 Phase Turbulence in a Convection Layer Rotating about a Vertical Axis

In the case of a rotating layer as shown in figure 1 the phase turbulence assumes a particularly simple form and the connection to a heteroclinic cycle

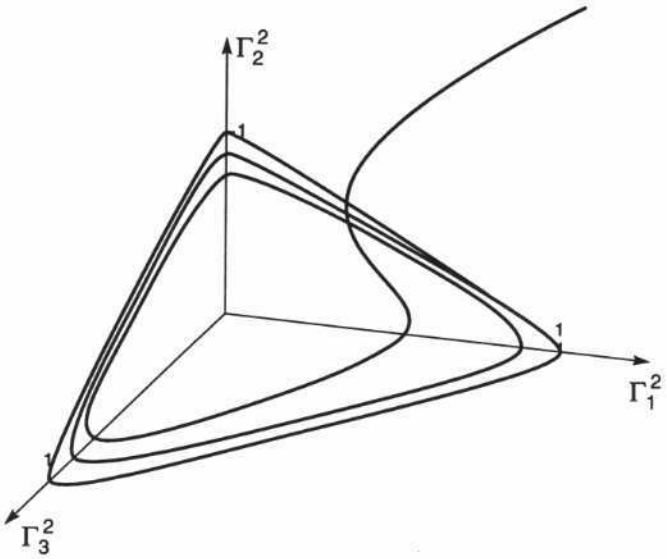

Fig. 2: Sketch of a trajectory in the phase space spanned by the amplitudes $\Gamma_i^2, i = 1, 2, 3$, which approaches the heteroclinic orbit connecting the fixed points $\Gamma_i^2 = \delta_{ij}$ with $j = 1, 2, 3$.

is most evident. As shown by Küppers and Lortz (1969), the growing disturbance of steady rolls, which is the only stable steady solution in the case $\beta = 0$, $\Omega < \Omega_c$, assumes the form of rolls oriented with an angle of about 60° with respect to the given rolls when Ω exceeds Ω_c. Because of this property it is sufficient to use a set of three rolls for a simple model of the time dependence of convection (Busse and Clever, 1979a). The corresponding evolution equations are

$$\begin{aligned} \tfrac{d}{d\tau}\Gamma_1 &= (1 - \Gamma_1^2 - \xi\Gamma_2^2 - \gamma\Gamma_3^2)\Gamma_1, \\ \tfrac{d}{d\tau}\Gamma_2 &= (1 - \Gamma_2^2 - \xi\Gamma_3^2 - \gamma\Gamma_1^2)\Gamma_2, \\ \tfrac{d}{d\tau}\Gamma_3 &= (1 - \Gamma_3^2 - \xi\Gamma_1^2 - \gamma\Gamma_2^2)\Gamma_3, \end{aligned} \tag{3.1}$$

where the variables Γ_n are rescaled versions of the amplitudes C_n and τ is identical with the time t except for a constant factor. Without losing generality we may assume real variables Γ_n. The system (3.1) of equations has eight fixed points all of which are unstable for $\gamma + \xi > 2$ when either $\gamma < 1$ or $\xi < 1$ holds. The same system (3.1) of equations was first used in the context of population biology by May and Leonard (1975) and some mathematical properties are discussed in their paper. ¿From arbitrary initial conditions the trajectory in the space spanned by coordinates $\Gamma_1^2, \Gamma_2^2, \Gamma_3^2$ approaches a heteroclinic cycle in the plane $\Gamma_1^2 + \Gamma_2^2 + \Gamma_3^2 = 1$ as indicated in figure 2.

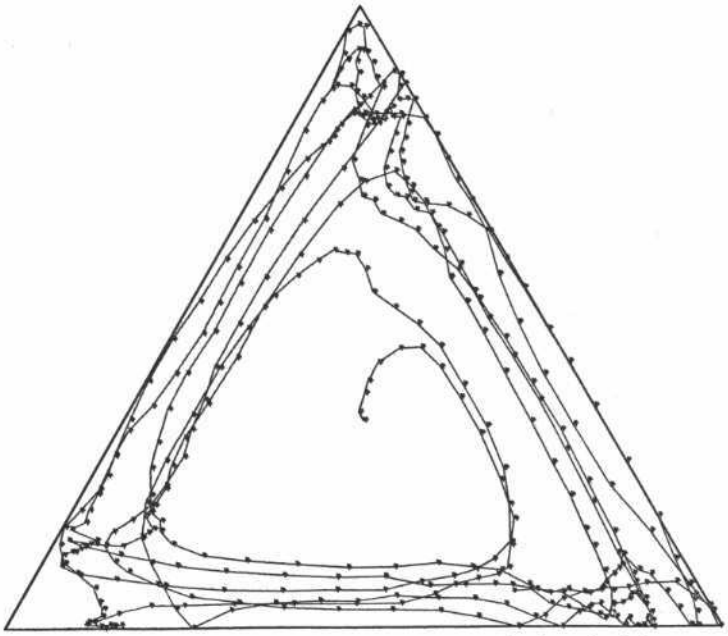

Fig. 3: Trajectory of the statistical limit cycle described by equations (3.1) with superimposed noise (see Busse, 1984) in the triangular domain given by the three corners $\Gamma_i^2 = \delta_{ij}, j = 1,2,3$. The trajectory starts at the unstable fixpoint $\Gamma_1 = \Gamma_2 = \Gamma_3$ in the center of the triangle. The stars are placed at equal time intervals.

As the heteroclinic cycle is approached the unphysical feature of an ever increasing period becomes apparent. In realistic situations the interaction of patches of rolls with varying orientations will create disturbances which will prevent the ultimate approach to the heteroclinic orbit. The effect of the disturbances can be modeled through the addition of noise in the system (3.1) of equations as was done by Busse (1984). A typical picture of the conversion of the heteroclinic cycle into a 'statistical limit cycle' is shown in figure 3. The average frequency of this cycle is proportional to

$$(R - R_c)(1 - \gamma)(\log(1/\eta))^{-1}$$

where $R - R_c$ is the excess of the Rayleigh number over its critical value, $1 - \gamma$ is proportional to the growth rate of the Küppers–Lortz instability in the case $\gamma < 1$ and η is a typical amplitude of the disturbances generated by white noise.

The statistical limit cycle concept is useful for the understanding of the local replacement of rolls by other rolls differing in their orientation by approximately 60° as seen in experiments with high Prandtl number fluids. An

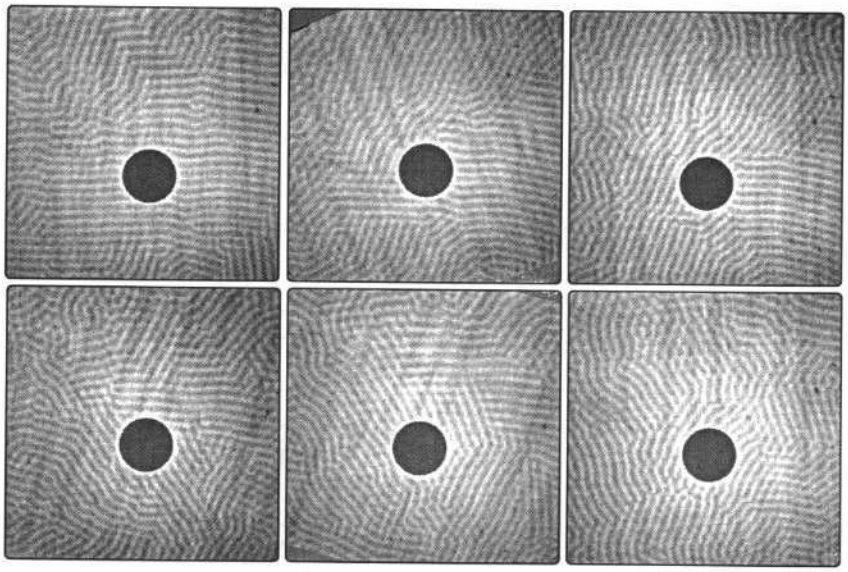

Fig. 4: Phase turbulent convection induced by the Küppers–Lortz instability in a horizontal layer of methyl alcohol of thickness d = 3.3mm rotating about a vertical axis. The shadowgraph pictures have been taken 2 minutes apart in the clockwise sequence (upper row left to right, then lower row right to left). The central circle originates from the cooling water channel at the top of the layer and does not interfere with the pattern dynamics. Rolls tend to be replaced by other rolls turned counterclockwise by about 60°. (For details see Heikes and Busse, 1980; Busse and Heikes, 1980.)

example from the work of Heikes and Busse (1980) is shown in figure 4. The disturbance amplitude η can be interpreted as the influence of neighboring patches and η^{-1} thus is roughly proportional to the size of the patches which increases as the critical Rayleigh number is approached. Through the inclusion of gradient terms in the system (3.1) non-local effects can be taken into account (Tu and Cross, 1992) and a statistical limit cycle can be found without the inclusion of noise. In the case of rotating convection layers with Prandtl numbers of the order of unity the angle between rolls and the most strongly growing disturbance rolls becomes smaller than 60° and the dynamics can no longer be described by as simple a system as (3.1). In spite of a smaller angle of the strongest growing disturbance a predominance of rolls differing by 60° in orientation can still be noticed in the experimental measurements (Hu *et al.*, 1995, 1998).

Heteroclinic cycles also play a role in the other case of phase turbulence

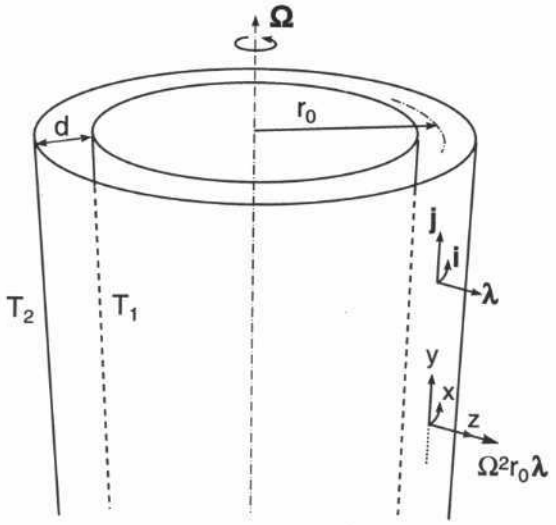

Fig. 5: Geometrical configuration of an annular convection layer with 'horizontal' axis of rotation.

occurring at the critical value of the Rayleigh number. A discussion of the dynamical features leading to phase turbulence in a convection layer with stress-free boundaries has been given by Busse *et al.* (1992). But, as has already been mentioned, a comparison between theory and experiment does not seem to be possible in this case.

4 Phase Turbulence in a Convection Layer with Horizontal Axis of Rotation

Another way of realizing buoyancy driven motions is to use the centrifugal force in place of gravity. By cooling an inner rotating cylinder and heating an outer co-rotating one a Rayleigh–Bénard convection layer is realized with the Rayleigh number given by

$$R = \frac{\gamma(T_2 - T_1)\Omega_D^2(r_1 + r_2)d^3}{2\nu\kappa}, \tag{4.1a}$$

where γ is the thermal expansivity, T_2 and T_1 are the temperatures at which the outer and inner cylindrical boundaries are kept and r_2 and r_1 are the corresponding radii, d is the gap width, $d = r_2 - r_1$, Ω_D is the rotation rate, ν is the kinematic viscosity and κ is the thermal diffusivity. A sketch of the geometrical configuration is shown in figure 5. There are two additional di-

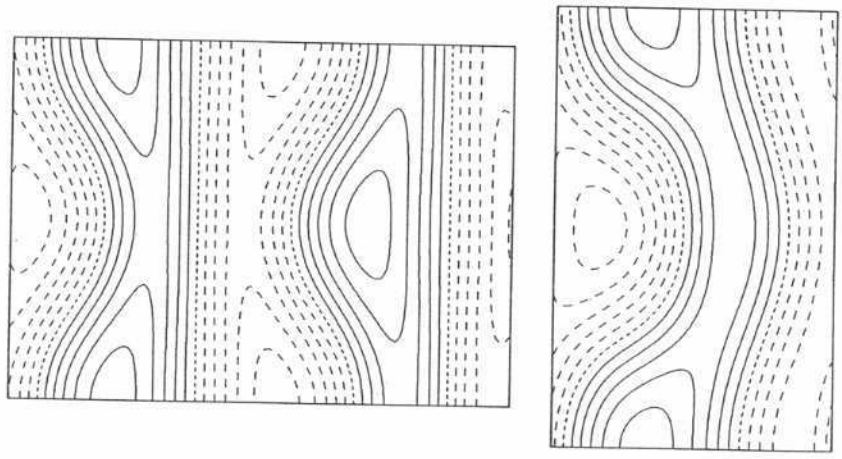

Fig. 6: Hexarolls (left) for $R = 2300$ with $\boldsymbol{k}_1 = (3.117, 0)$, $\boldsymbol{k}_{2,3} = (-1.559, \pm 2.2)$ and knot convection (right) for $R = 2400$ with $\boldsymbol{k}_1 = (3.117, 0)$, $\boldsymbol{k}_2(0, 2.2)$. $P = 1000, \Omega = 20$ in both cases. Solid (dashed) lines indicate positive (negative) isotherms in the midplane $z = 0$ of the fluid layer.

mensionless parameters, the rotation parameter Ω and the Prandtl number P,

$$\Omega = \Omega_D d^2/\nu, \qquad P = \frac{\nu}{\kappa}, \tag{4.1b}$$

if we restrict our attention to the small gap limit, $d \ll r_1$. The idea is to minimize the effect of the Coriolis force by keeping Ω small while making the centrifugal force sufficiently large that it exceeds gravity by a good margin. This constraint can be satisfied for laboratory experiments through the use of high Prandtl number fluids such as highly viscous silicone oils.

On the theoretical side the assumption of a small Ω permits the consideration of the problem as an unfolding from the bifurcation with infinite codimension in the isotropic limit of $\Omega = 0$. We can thus use the formulation of the problem (2.1), (2.2) and restricting ourselves to the case of rigid boundaries with $\beta = 0$ we arrive at the equations

$$\begin{aligned} \frac{d}{dt} C_l^+ &= (R - R_c - \tau^2 (\boldsymbol{k}_l \cdot \boldsymbol{j})^2 \alpha^{-2}) K C_l^+ - \sum_{n=1}^{N} |C_n|^2 A (\boldsymbol{k}_l \cdot \boldsymbol{k}_n) C_l^+ \\ &\quad + i\Omega \sum_{n,m=-N}^{N} \delta(\boldsymbol{k}_l + \boldsymbol{k}_n + \boldsymbol{k}_m) B C_n C_m (\boldsymbol{k}_n \times \boldsymbol{k}_m \cdot \boldsymbol{\lambda}) \boldsymbol{j} \cdot \boldsymbol{k}_n, \end{aligned} \tag{4.2}$$

where B is a constant as long as the absolute values of the $\boldsymbol{k}$-vectors are constant. Equations (4.2) admit the familiar roll solutions corresponding to

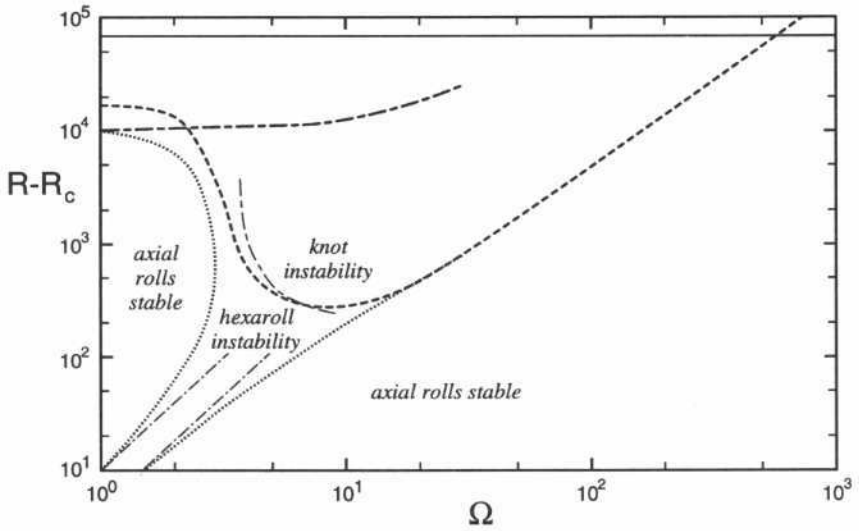

Fig. 7: Regions in the R-Ω-plane where axial rolls are stable or unstable with respect to the indicated instabilities for $P = 7$.

$N = 1$. Among these the axially oriented rolls corresponding to $\boldsymbol{k}_1 \cdot \boldsymbol{j} = 0$ are preferred since the Ω-dependence vanishes for these rolls. The unusual last term of equations (4.2) gives rise to new instabilities and new forms of three-dimensional convection flows. An example of the latter are the hexarolls which are shown in figure 6. They have been derived by Auer *et al.* (1995) in the case $N = 3$ with $\boldsymbol{k}_1 \cdot \boldsymbol{j} = 0$ and $\boldsymbol{k}_1 + \boldsymbol{k}_2 + \boldsymbol{k}_3 = 0$. Another form of three-dimensional convection is knot convection. This type of convection can be observed in a non-rotating Rayleigh–Bénard layer (Busse and Clever, 1979b) and has also been investigated numerically (Clever and Busse, 1989). In the present case of a convection layer with horizontal axis of rotation, knot convection occurs at much lower values of the Rayleigh number so that the analysis of the weakly nonlinear limit applies. Auer *et al.* (1995) have shown that the description of knot convection based on equations (4.2) in the case $N = 2$ agrees well with the numerical solutions of the full equations. A plot of knot convection is also given in figure 6. A diagram indicating the regions of the R-Ω-plane where axial rolls are stable and where they are unstable with respect to the hexaroll and knot instabilities is given in figure 7.

The hexaroll instability leads to the evolution of stable steady hexarolls only in a small fraction of the unstable region. For small values of $R - R_c$ the hexarolls are also unstable and a nearly heteroclinic cycle results (Busse and Clever, 1999). It manifests itself in the form of the long period oscillation shown in figure 8. Axial rolls described by $\boldsymbol{k}_1$ become unstable with respect

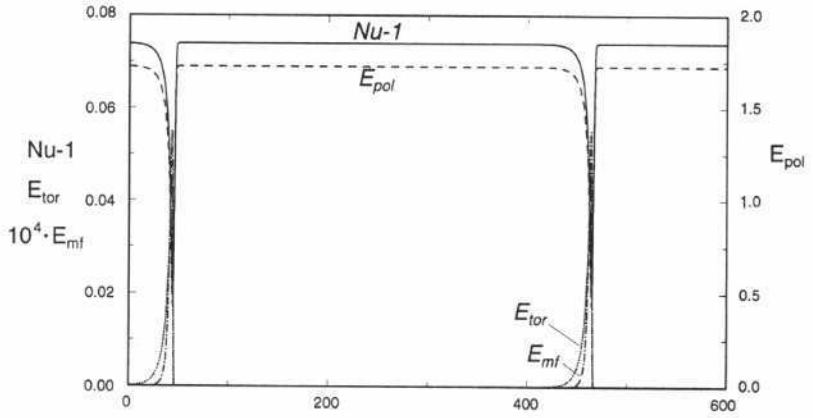

Fig. 8: Nearly heteroclinic cycle between axial rolls 180° out of phase with the brief changeover induced by the hexaroll instability. The energies E_{pol}, E_{tor} and E_{mf} of the poloidal and toroidal components of the velocity field and of the mean flow have been plotted as functions of time. Also shown is the Nusselt number Nu in dependence on t. Hexaroll convection is characterized by a finite toroidal component and by a finite mean x-component of the velocity field both of which vanish in the case of axial rolls.

to the hexaroll instability, the amplitudes C_2, C_3 corresponding to $\boldsymbol{k}_2, \boldsymbol{k}_3$ with $\boldsymbol{k}_1 + \boldsymbol{k}_2 + \boldsymbol{k}_3 = 0$ grow while C_1 decays to zero. But a new steady state can not be attained. Instead C_1 changes sign and axial rolls 180° out of phase with the original one become established until after many thermal diffusion times the hexaroll disturbances grow again. The switch over can be seen in the time sequence of plots of figure 9. For the analysis of convection it is convenient to use the decomposition of the velocity field $\boldsymbol{u}$ into poloidal and toroidal components, and into its mean component $\boldsymbol{U}$ which represents the average of $\boldsymbol{u}$ over the x-y-plane,

$$\boldsymbol{u} = \nabla \times (\nabla\varphi \times \boldsymbol{\lambda}) + \nabla\psi \times \boldsymbol{\lambda} + \boldsymbol{U}, \tag{4.3}$$

where the condition can be imposed that the x-y-average of the functions φ and ψ vanishes. Axial rolls are characterized by the property $\psi \equiv 0$ while all other solutions exhibit a toroidal function ψ proportional to Ω. The results are essentially independent of the Prandtl number P as soon as P exceeds order 10. The time scale of all dynamic processes is the thermal diffusion time, d^2/κ, where κ is the thermal diffusivity.

Considerable efforts have been expended to realize the interesting dynamics of a convection layer with parallel axis of rotation in the laboratory (Jaletzky and Busse, 1998; Jaletzky, 1999). A sketch of the apparatus is given in those papers. It represents a realization of the configuration of figure 5 with

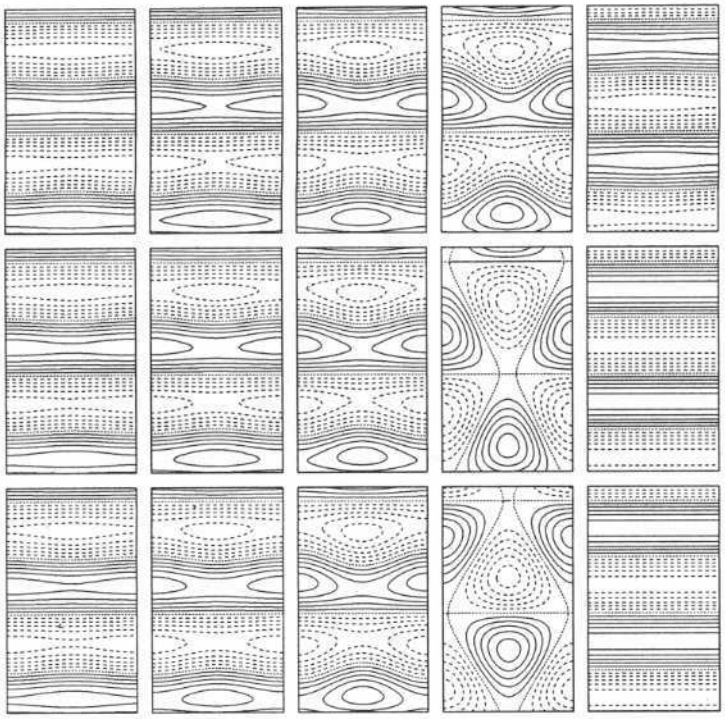

Fig. 9: Time sequence of plots $\Delta t = 4$ apart ($\Delta t = 2$ for the last five intervals), from top to bottom then left to right, in the transition regime when axial rolls become unstable to the hexaroll instability and convection returns to axial rolls 180° out of phase with the original ones. The plots show lines of constant temperature in the midplane of the layer for $R = 1800, \Omega = 5, P = 7$. The wavenumber in the x-direction (upwards) is $2.7d^{-1}$ and in the y-direction (towards the right) it is $1.559d^{-1}$ (after Busse and Clever, 1999.)

vertical axis such that laboratory gravity does not give rise to an oscillatory force. It has been possible to generate both hexaroll convection and knot convection, as shown in figure 10. Through the use of highly viscous fluids it is possible to achieve low values of Ω, while the centrifugal acceleration exceeds that of gravity by as much as a factor of 10. Thermochromatic liquid crystals embedded in thin plastic sheets and attached to the inner cylinder have been used for visualization. As shown in the photographs of figure 10, hexaroll convection and knot convection can be observed in accordance with the theory. At higher Rayleigh numbers oblique rolls predominate which have not been considered in the theoretical analysis of Auer *et al.* (1995). Unfortunately, it has not yet been possible to observe experimentally the

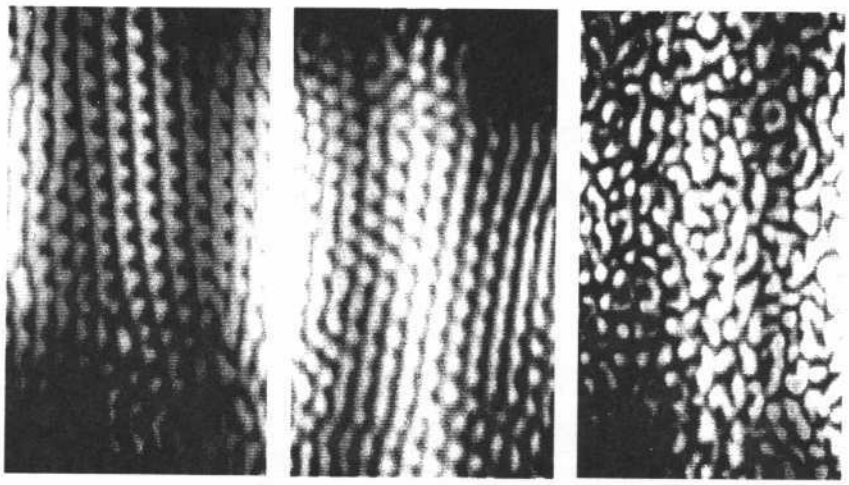

Fig. 10: Hexaroll convection at $R = 2300, \Omega = 10$ (middle), knot convection at $R = 4880, \Omega = 24$ (left) and phase turbulent convection at $R = 3970, \Omega = 14$ (right) observed in a rotating cylindrical annulus as sketched in figure 5. $P \approx 400$ and rotation is clockwise in all three cases.

phase turbulence arising from the existence of the nearly heteroclinic cycle shown in figures 8 and 9. Since this cycle seems to be confined to a region of less than 10% above the critical value of the Rayleigh number it can not easily be visualized. The amplitude of the temperature variations induced by convection is too weak in this regime to induce a visible change of color of the liquid crystals.

It is possible, however, to carry out numerical simulations based on computer code developed by Pesch (1996). An example of these simulations is shown in figure 11 where the intermittent appearance of hexaroll convection is clearly visible. It can also be seen that the phase of the two-dimensional axial rolls changes by 180° as they reappear after the hexaroll episode. The numerical simulations can be run for extended periods in time and the statistical properties of the phase turbulence can be analyzed as functions of the parameters of the problem. As must be expected on the basis of the analysis of the spatially periodic convection displayed in figures 8 and 9 the phase turbulent convection becomes purely time periodic in the case of low aspect ratio layers when the coherence length of patches of hexaroll convection becomes comparable to the horizontal periodicity interval.

The numerical simulation can also be employed to describe the phase turbulent convection at higher Rayleigh numbers as seen in the third picture of figure 10. A typical time sequence of the spatio-temporally chaotic state is

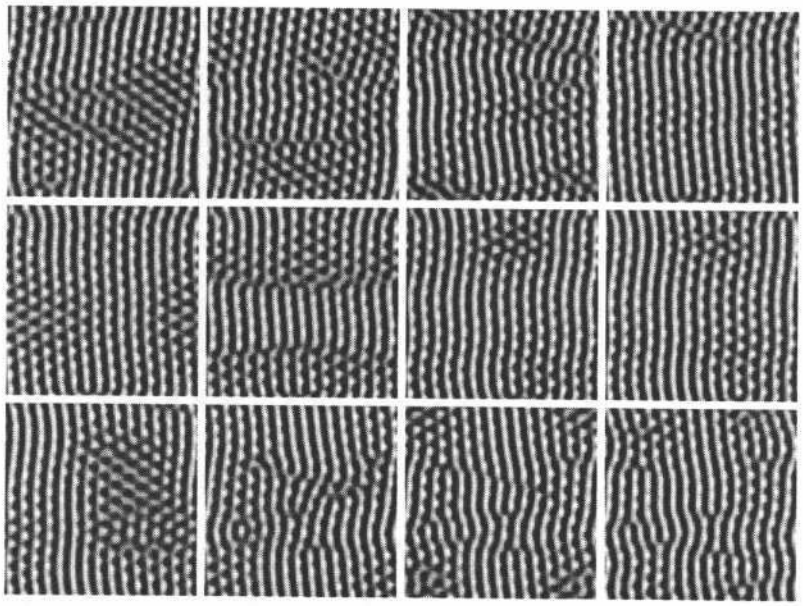

Fig. 11: Time sequence of plots (left to right, then top to bottom) with $\Delta t = 14$ showing the normal velocity in the midplane of the layer in the case of phase turbulence induced by the hexaroll instability of axial rolls in the case $R = 1814, \Omega = 5, P = 10$. The shift of the rolls by 180° after the hexaroll interlude is clearly visible.

shown in figure 12 which resembles the experimental observation in figure 10. It is of interest to note that an oscillation in which the axial roll component switches phase by 180° is still noticeable. A full period corresponds to about 1.6 thermal time units so that after four pictures in figure 12 vertical line segments have switched from black to white or vice versa. A quantitative measure of this chaotic switching phenomenon can be obtained from the correlation between patterns at the times t_0 and $t_0 + t$. As a typical example the correlation averaged over t_0 for the pattern of the vertical velocity has been plotted in figure 13. The period evident in this figure appears to be a remnant of the heteroclinic cycle. Attempts to measure the correlation experimentally are under way. Preliminary results appear to be consistent with the numerical results.

5 Concluding Remarks

In this article we have focused on systems where the phenomenon of phase turbulence is related to heteroclinic cycles. It is an open question whether similar mechanisms operate in other situations as well. The absence of a Lyapunov

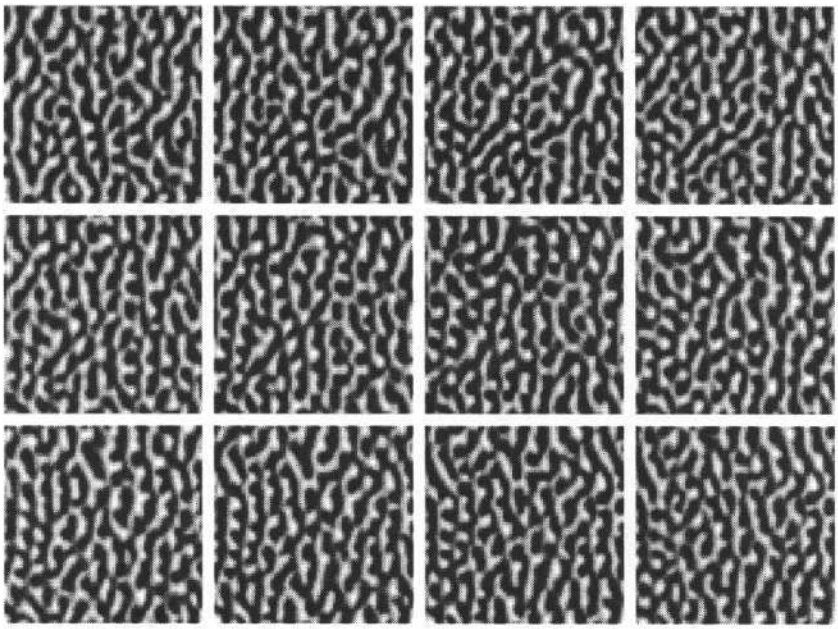

Fig. 12: Time sequence of plots (left to right, top to bottom) with $\Delta t = 0.2$ showing the normal velocity in the midplane of the layer in the case $R = 3440, \Omega = 15, P = 10$. The phase of the axial roll component still appears to switch by 180° about every fourth plot.

potential is a necessary condition for complex spatio-temporal dynamics, but not a sufficient one. High Prandtl number convection in a non-rotating layer, for instance, shows little time dependence even at 10 times the critical value of the Rayleigh number.

In the case of convection with stress-free boundaries a Lyapunov potential does not exist owing to the presence of the mean-flow mode. This mode can be understood as a Goldstone mode originating from the spontaneously broken (continuous) Galilean invariance. Since such modes are only weakly damped they can easily be excited by any small perturbations in the patterns, which are then typically reinforced. Phase turbulence in liquid crystals is closely related to this mechanism. Here a Goldstone mode with respect to the orientational degrees of freedom comes into play (Rossberg *et al.*, 1996).

Even less well understood is the phenomenon of spiral-defect chaos in convection layers with Prandtl numbers of the order of unity. It seems that here a kind of wave vector frustration is important. The different building blocks of the patterns (spirals, grain boundaries etc.) select different wave vectors and the system is unable to reconcile those into a stationary periodic pattern

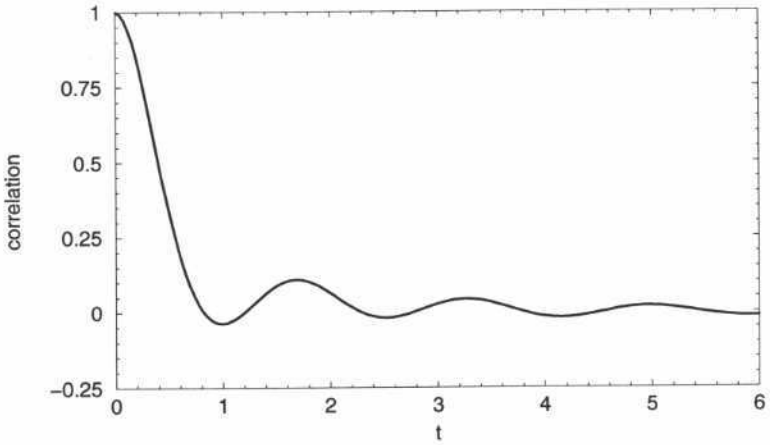

Fig. 13: Correlation function $\int w(t_0)w(t_0+t)dxdy$ averaged over t_0 in the range $0 < t_0 < 400$ as a function of t, for the parameters of figure 12; w denotes the normal component of the velocity at the midplane of the layer.

(Cakmur *et al.*, 1997).

References

Auer, M., Busse, F.H., and Clever, R.M. (1995) 'Three-dimensional convection driven by centrifugal buoyancy', *J. Fluid Mech.* **301**, 371–382.

Bodenschatz, E., Cannell, D.S., de Bruyn, J.R., Ecke, R., Hu, Y.-C., Lerman, K. and Ahlers, G. (1992) 'Experiments on three systems with non-variational aspects', *Physica D* **61**, 77–93.

Busse, F.H. (1967) 'The stability of finite amplitude cellular convection and its relation to an extremum principle', *J. Fluid Mech.* **30**, 625–649.

Busse, F.H. (1978) 'Nonlinear properties of convection', *Rep. Progress in Physics* **41**, 1929–1967.

Busse, F.H. (1984) 'Transition to turbulence via the statistical limit cycle route', in *Turbulence and Chaotic Phenomena in Fluids*, T. Tatsumi, ed., Elsevier, pp. 197–202.

Busse, F.H. (1986) 'Phase-turbulence in convection near threshold', *Contemp. Math.* **56**, 1–8.

Busse, F.H. and Bolton, E.W. (1984) 'Instabilities of convection rolls with stress-free boundaries near threshold', *J. Fluid Mech.* **146**, 115–125.

Busse, F.H. and Clever, R.M. (1979a) 'Nonstationary convection in a rotating system', in *Recent Developments in Theoretical and Experimental Fluid Mechanics*, U. Müller, K.G. Roesner and B. Schmidt, eds., Springer, pp. 376–385.

Busse, F.H. and Clever, R.M. (1979b) 'Instabilities of convection rolls in a fluid of moderate Prandtl number', *J. Fluid Mech.* **91**, 319–335.

Busse, F.H. and Clever, R.M. (1999) 'Heteroclinic cycles and phase turbulence', in *Pattern Formation in Continuous and Coupled Systems*, M. Golubitsky, D. Luss and S. Strogatz, eds., IMA Volumes in Mathematics and its Applications, vol. 115, Springer, pp. 25–32.

Busse, F.H. and Heikes, K.E. (1980) 'Convection in a rotating layer: a simple case of turbulence', *Science* **208**, 173–175.

Busse, F.H., Kropp, M. and Zaks, M. (1992) 'Spatio-temporal structures in phase-turbulent convection', *Physica D* **61**, 94–105.

Busse, F.H. and Sieber, M. (1991) 'Regular and chaotic patterns of Rayleigh–Bénard convection', in *Bifurcation and Chaos: Analysis, Algorithms, Applications*, R. Seydel, F.W. Schneider, T. Küppers and H. Troger, eds., Birkhäuser, pp. 75–88.

Cakmur, R.V., Egolf, D.A., Plapp, B.B. and Bodenschatz, E. (1997) 'Bistability and competition of spatiotemporal chaotic and fixed point attractors in Rayleigh–Bénard convection', *Phys. Rev. Lett.* **79**, 1853–1856.

Clever, R.M. and Busse, F.H. (1989) 'Three-dimensional knot convection in a layer heated from below', *J. Fluid Mech.* **198**, 345–363.

Dangelmayr, G. and Kramer, L. (1998) 'Mathematical tools for pattern formation', in *Evolution of Spontaneous Structures in Dissipative Continuous Systems*, F.H. Busse and S.C. Müller, eds., Springer Lecture Notes in Physics, vol. M55, pp. 1–85.

Fantz, M., Friedrich, R., Bestehorn, M. and Haken, H. (1992) 'Pattern formation in rotating Bénard convection', *Physica D* **61**, 147–154.

Goldstein, R.J. and Graham, D.J. (1969) 'Stability of a horizontal fluid layer with zero shear boundaries', *Phys. Fluids* **12**, 1133–1137.

Heikes, K.E. and Busse, F.H. (1980) 'Weakly nonlinear turbulence in a rotating convection layer', *Ann. NY Acad. Sci.***357**, 28–36 .

Hu, Y., Ecke, R.E. and Ahlers, G. (1995) 'Time and length scales in rotating Rayleigh–Bénard convection', *Phys. Rev. Lett.* **74**, 5040–5043.

Hu, Y., Ecke, R.E. and Ahlers, G. (1997) 'Convection under rotation for Prandtl numbers near 1: linear stability, wavenumber selection and pattern dynamics', *Phys. Rev. E* **55**, 6928–6949.

Hu, Y., Pesch, W., Ahlers, G. and Ecke, R.E. (1998) 'Convection under rotation for Prandtl numbers near 1: Küppers–Lortz instability', *Phys. Rev. E* **58**, 5821–5833.

Jaletzky, M. (1999) 'Über die Stabilität von thermisch getriebenen Strömungen im rotierenden konzentrischen Ringspalt', Dissertation, University of Bayreuth.

Jaletzky, M. and Busse, F.H. (1998) 'New patterns of convection driven by centrifugal buoyancy', *ZAMM* **78**, S525–S526.

Küppers, G. and Lortz, D. (1969) 'Transition from laminar convection to thermal turbulence in a rotating fluid layer', *J. Fluid Mech.* **35**, 609–620.

May, R.M. and Leonard, W.J. (1975) 'Nonlinear aspects of competition between three species', *SIAM J. Appl. Math.* **29**, 243–253.

Mielke, A. (1997) 'Mathematical analysis of sideband instabilities with application to Rayleigh–Bénard convection', *J. Nonlinear Sci.* **7**, 57–99.

Millán-Rodríguez, J., Bestehorn, M., Pérez-García, C., Friedrich, R. and Neufeld, M. (1995) 'Defect motion in rotating fluids', *Phys. Rev. Lett.* **74**, 530–533.

Morris, S.W., Bodenschatz, E., Cannell, D.S. and Ahlers, G. (1993) 'Spiral defect chaos in large aspect ratio Rayleigh–Bénard convection', *Phys. Rev. Lett.* **71**, 2026–2029.

Neufeld, M. and Friedrich, R. (1995) 'Statistical properties of the heat transport in a model of rotating Bénard convection', *Phys. Rev. E* **51**, 2038–2045.

Pesch, W. (1996) 'Complex spatio-temporal convection patterns', *CHAOS* **6**, 348–357.

Pesch, W. and Behn, U. (1998) 'Electrohydrodynamic convection in nematics', in *Evolution of Spontaneous Structures in Dissipative Continuous Systems*, F.H. Busse and S.C. Müller, eds., Springer Lecture Notes in Physics, vol. M55, pp. 335–383.

Ponty, Y., Passot, T. and Sulem, P.L. (1997) 'Chaos and structures in rotating convection at finite Prandtl number', *Phys. Rev. Lett.* **79**, 71–74.

Rossberg, A.G., Hertrich, A., Kramer, L. and Pesch, W. (1996) 'Weakly nonlinear theory of pattern-forming systems with spontaneously broken isotropy', *Phys. Rev. Lett.* **76**, 4729–4732.

Tu, Y. and Cross, M.C. (1992) 'Chaotic domain structure in rotating convection', *Phys. Rev. Lett.* **69**, 2515–2518.

Xi, H.-W., Li, X.-J. and Gunton, J.D. (1997) 'Direct transition to spatiotemporal chaos in low Prandtl number fluids', *Phys. Rev. Lett.* **78**, 1046–1049.

Zhong, F., Ecke, R. and Steinberg, V. (1991) 'Rotating Rayleigh–Bénard convection: Küppers–Lortz transition', *Physica D* **51**, 596–607.

Zhong, F. and Ecke, R.E. (1992) 'Pattern dynamics and heat transport in rotating Rayleigh–Bénard convection', *CHAOS* **2**, 163.

Zippelius, A. and Siggia, E.D. (1982) 'Disappearance of stable convection between free-slip boundaries', *Phys. Rev. A* **26**, 1788–1790.